

# “Steric armor” strategy of blue fluorescent emitters to against photooxidation-induced degradation

Sha-Sha Wang<sup>1</sup>, Jing-Rui Zhang<sup>1</sup>, Kuan-De Wang<sup>1</sup>, Hao-Ran Li<sup>1</sup>, Peng-Hui Meng<sup>1</sup>, Yang Zhou<sup>1</sup>, xiang yu<sup>1</sup>, Ying Wei<sup>1</sup>, Quan-You Feng<sup>1</sup>, Yu-He Kan<sup>2</sup>, and Linghai Xie<sup>1</sup>

<sup>1</sup>Nanjing University of Posts and Telecommunications

<sup>2</sup>Huaiyin Normal University

January 30, 2024

## Abstract

Stability against oxygen is an important factor affecting the performance of organic semiconductor devices. Improving photooxidation stability can prolong the service life of the device and maintain the mechanical and photoelectric properties of the device. Generally, various encapsulation methods from molecular structure to macroscopic device level are used to improve photooxidation stability. Here, we adopted a crystallization strategy to allow 14H-spiro[dibenzo[c,h]a-cridine-7,9'-uorene] (SFDBA) to pack tightly to resist fluorescence decay caused by oxidation. In this case, the inert group of SFDBA acts as a “steric armor”, protecting the photosensitive group from being attacked by oxygen. Therefore, compared with the fluorescence quenching of SFDBA powder under two hours of sunlight, SFDBA crystal can maintain its fluorescence emission for more than eight hours under the same conditions. Furthermore, the photoluminescence quantum yields (PLQYs) of the crystalline film is 327.37 % higher than that of the amorphous film. It shows that the crystallization strategy is an effective method to resist oxidation.

**Cite this paper:** *Chin. J. Chem.* **2023**, *41*, XXX–XXX.

**DOI:** 10.1002/cjoc.202300XXX

“Steric armor” strategy of blue fluorescent emitters to against photooxidation-induced degradation

Sha-Sha Wang,<sup>a</sup> Jing-Rui Zhang,<sup>a</sup> Kuan-De Wang,<sup>a</sup> Hao-Ran Li, <sup>a</sup>Peng-Hui Meng, <sup>a</sup> Yang Zhou, <sup>a</sup> Xiang Yu, <sup>a</sup> Ying Wei,<sup>a</sup> Quan-You Feng,<sup>\*,a</sup> Yu-He Kan,<sup>\*,b</sup> and Ling-Hai Xie<sup>\*,a</sup>

<sup>a</sup> Centre for Molecular Systems and Organic Devices (CMSOD), State Key Laboratory of Organic Electronics and Information Displays & Institute of Advanced Materials, Jiangsu National Synergetic Innovation Center for Advanced Materials (SICAM), Nanjing University of Posts & Telecommunications, Nanjing, Jiangsu 210023, China<sup>b</sup> Jiangsu Key Laboratory for Chemistry of Low-Dimensional Materials, Huaiyin Normal University, Huaian, Jiangsu, 223300, China

---

## Keywords

Organic semiconductor | Photooxidation | Spirocyclic aromatic hydrocarbons | Crystal engineering | Fluorescence

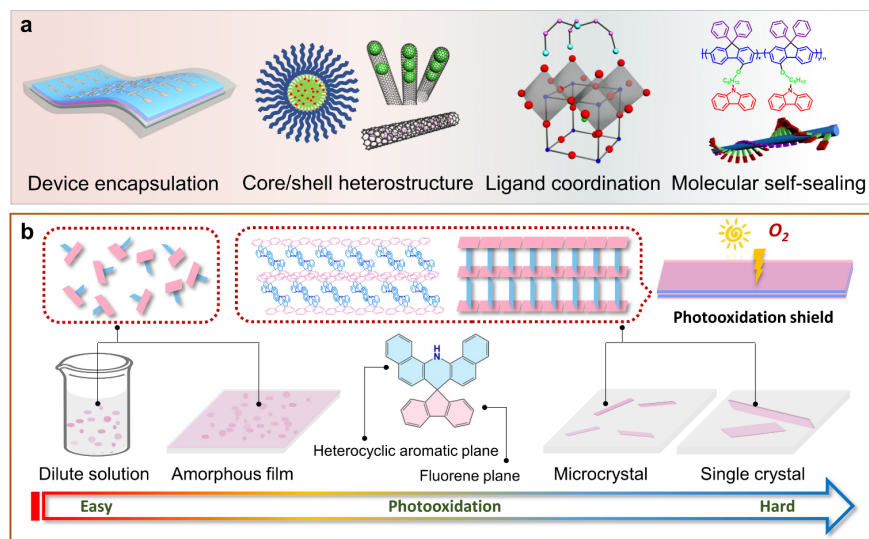
## Comprehensive Summary

Stability against oxygen is an important factor affecting the performance of organic semiconductor devices. Improving photo

---

## Background and Originality Content

Stability against oxygen is of great importance in the practical applications of organic semiconductor materials, considering the functional groups with high photoelectric activity are particularly sensitive to oxygen when excited by light and electricity.<sup>[1-2]</sup> The adverse effects of unstable organic semiconductors as shortened service lifetime, deteriorative mechanical property and optoelectronic performance are ubiquitous in various single-molecular and hybrid systems which must work under ambient conditions, including integrated photovoltaic,<sup>[3-4]</sup> fluorescence imaging,<sup>[5-7]</sup> organic light emitting diode (OLED),<sup>[8]</sup> and organic field-effect transistors (OFET).<sup>[9]</sup> To inhibit the degradation, several kinds of additives such as light screeners/absorbers, excited-state quenchers, antioxidants, radical scavengers have been developed according to different stabilization mechanisms. Whereas for organic semiconductors, the purity requirements are very severe to avoid the low efficiency owing to the defect role of additive molecules. Besides, customization of the molecular structures was proved effective for the enhancement of stability, like replacing the covalent bonds with low bond dissociation energy,<sup>[10]</sup> adding electron withdrawing groups to increase the oxidation potentials<sup>[11]</sup> and so on. However, in many cases the molecular design of electronic structure is not enough to meet the functional and stability requirements at the same time.



Despite the above efforts, a complementary and alternative methodology is to create an environment to insulate the active groups from the oxygen molecules. According to this idea, encapsulation technology has been developed in numerous applications to improve the stability of materials and devices spanning from macro- to nano-levels, as concluded in Figure 1a.<sup>[12-17]</sup> For instance, device encapsulation is an indispensable procedure in the fabrication of OLED, which incorporates glass or metal cover sealed with ultraviolet (UV)-cured epoxy resin, multilayer thin films of polymers, and metal complexes by deposition technologies.<sup>[18]</sup> The strategy of encapsulation is so powerful that have been applied from the hermetic packaging of macroscopic devices to the microscopic molecules or nanoparticles in many areas such as catalysts and drug delivery.<sup>[19-20]</sup> The related numerous coating materials involve host macrocycles,<sup>[21]</sup> cross-linked copolymers,<sup>[22-25]</sup> and carbon materials.<sup>[26]</sup> Besides these coatings, groups of molecules can also act as the barriers and exhibit a self-encapsulation effect. Conjugated polymer polydiarylfuorene (PHDPF-Cz) shows an excellent single-chain featured emission, which is attributed to the defense of polymer backbone by the  $\pi$ - $\pi$  stacking encapsulation of carbazole side group,<sup>[17]</sup> inspired a novel encapsulation method in term of molecular design.

Herein, we demonstrate an encapsulation paradigm to dramatically increase the stability of oxygen-sensitive

blue fluorescent emitters via a “steric armor” strategy as shown in Figure 1b. The model molecule *14H-spiro[dibenzo[*c,h*]a-cridine-7,9'-uorene]* (SFDBA) in amorphous state tends to be oxidized within 2 h under sunlight irradiation, while SFDBA crystals sheltered by the closely packed fluorenyl defense are able to remain the same under sunlight irradiation for 8 h. The self-encapsulation packing is due to the well-designed bi-planar cruciform-shaped molecular structure. The effective stability strategy is due to two interrelated reasons: one is the insulation of active naphthylamine groups away from oxygen by inert fluorenyl groups as sterically hindered walls; the other is the low-dimensional morphology further maximization the exposed plane paved by the fluorenyl walls. Furthermore, the photo-

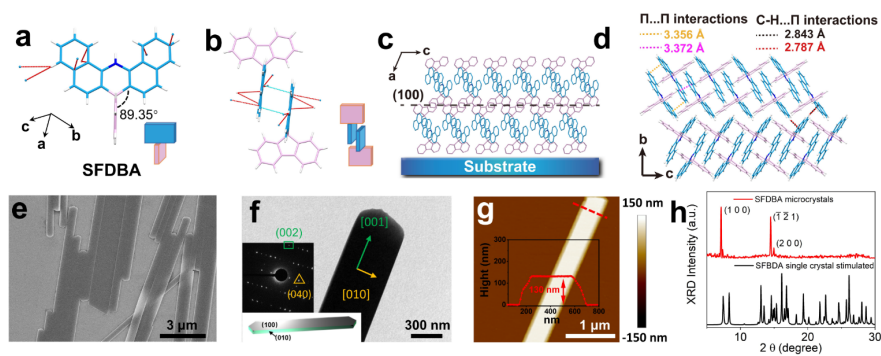
**Figure 1** The comparison between previous encapsulation methods and the crystallization strategy. a) Encapsulation examples with different scales and package modes including macroscopic device encapsulation, microscopic core/shell heterostructure, ligand coating and self-sealing of single molecule. b) Schematic representation exhibits the distinct photooxidation stabilities of different aggregation states, which is closely related to the SFDBA molecular arrangements.

luminescence quantum yields (PLQYs) of microcrystal films increase by 48.18 % and 327.37 % compared with solutions and amorphous films. This work provides an ingenious example for the rational noncovalent interaction design of molecule which leads the favorable molecular arrangement to enhance the oxidative stability and luminescence.

## Results and Discussion

SFDBA is a typical spirocyclic molecule which can be deemed as a combination of a heterocyclic aromatic plane and a fluorene plane as shown in Figure 1b. Naphthylamine group in the heterocyclic aromatic plane is oxygen-sensitive under sunlight irradiation, thus SFDBA should be freshly synthesized through the one-pot synthesis and characterized by  $^1\text{H}$  NMR in Figure S1 (Supporting Information, SI), then keep away from light and oxygen. To explore the influence of crystallization on the photooxidation process, single crystals and microcrystals of SFDBA were cultivated. Single crystals of SFDBA were prepared via solvent diffusion and the growth condition is listed in Table S1. The single crystal data in Table S2 indicate that the SFDBA crystal is assigned to monoclinic space group of  $P 2_1/c$ , with cell parameters of  $a = 12.293 \text{ \AA}$ ,  $b = 23.528 \text{ \AA}$ ,  $c = 7.576 \text{ \AA}$ ,  $\alpha = 90^\circ$ ,  $\beta = 104.476^\circ$ ,  $\gamma = 90^\circ$ . The crystal molecular structure and the corresponding schematic diagram are illustrated in of Figure 2a, revealing a bi-planar cross-shaped conformation with a dihedral angle of  $89.35^\circ$ . For SFDBA, all the sites of supramolecular interactions are found in the heterocyclic plane with larger conjugate area. As demonstrated in our previous work,<sup>[27]</sup> the concentrated distribution of supramolecular weak interaction sites in the heterocyclic plane would make it attractive and tend to link with other heterocyclic planes, while the chemically stable fluorene planes line up on both sides. A dimer in Figure 2b expresses this interdigital lipid bilayer-like (ILB) packing mode, which signify layer-by-layer structures as revealed in Figure 2c. Viewed from  $b$ -axis, the ILB units arrange along  $c$ -axis to form an ILB chain, while the lack of adequate supramolecular forces between the upper and lower chains along  $a$ -axis (Figure S2) would contribute to the growth suppression of this direction and lead to the exposure of (100) plane. Figure 2d shows the perspective of the ILB chains in (100) plane as a single layer, revealing that the non-covalent interactions intrachain are  $\pi$ - $\pi$  interactions (distances of 3.356 and 3.372  $\text{\AA}$ ) and interchain are relatively weak C-H... $\pi$  interactions (distances of 2.843 and 2.787  $\text{\AA}$ ). The corresponding interaction energies (IE) (Table S3) within these molecules further indicate that the binding interaction of intrachain molecules along  $c$ -axis is the strongest, followed by the intrachain molecules along  $b$ -axis, and the interlayer along  $a$ -axis is the weakest. As a result, the prepared microcrystals are verified to exhibit a one-dimensional (1D) belt-like morphology using scanning electron microscopy (SEM), transmission electron microscopy (TEM) and atomic force microscopy (AFM) characterizations. Uniform SFDBA microcrystals with long strip shapes can be easily formed by reprecipitation without any additives as the SEM image disclosed in Figure 2e. Figure 2f show the TEM image of an individual SFDBA microcrystal with evident selected-area electron diffraction (SAED) dots (inset in Figure 2f, upper left) identified as (002) and (040). The crystal orientations of [001] and [010] are also indicated in the microcrystal. The cartoon model of SFDBA microcrystal (inset in Figure 2f, bottom left) exhibits two major crystal faces of (100) and (010). The height profile of a SFDBA microcrystal

in Figure 2g indicates a thickness of about 130 nm. The average length: width proportion is about 33:1 (16.5  $\mu\text{m}$  in length, 0.5  $\mu\text{m}$  in width) for SFDBA microcrystals from the size statistics in Figure S3. Moreover, the attachment energies of SFDBA crystal faces calculated by Materials Studio further confirm that the most thermodynamically stable crystal faces are  $\{100\}$  due to the lowest attachment energy (Table S4).<sup>[28]</sup> X-ray powder diffraction (XRD) patterns of SFDBA microcrystals in Figure 2h are completely in conformity with the SFDBA single crystals, and the strong  $\{100\}$  peaks parallel to the substrate represent the layer-by-layer structure of SFDBA microcrystals.



To disclose the effect of molecular arrangement on oxidation stability, solar experiments were performed on SFDBA in three different aggregation states under sunlight for different irradiation times. The corresponding photoluminescence (PL) spectra and digital photos of the samples under UV illumination are shown in Figure 3a-c. With the sunshine duration increasing, the emission peaks of SFDBA in dilute solutions become wider and shift from the initial 420 nm to 429 nm, 483 nm, 547 nm, 556 nm, indicating the complicated composition of the oxidation intermediates and products (Figure 3a). The changes in the emitting color from the digital

**Figure 2** The molecular structure, arrangement, and morphology analysis of SFDBA microcrystals. a) The crystal molecular structure of SFDBA. b) An interdigital lipid bilayer-like dimer. c) Layer-by-layer arrangements of SFDBA molecules viewed from  $b$ -axis. d) The molecular arrangements and supramolecular interactions in  $bc$ plane. e) SEM, f) TEM, and g) AFM images of SFDBA microcrystals. Inset in (f): in upper left is the corresponding SAED pattern performed from  $[100]$  zone-axis; in bottom left is the cartoon diagram of the microcrystal with two major crystal faces indexed. Inset in (g): the cross-sectional profile of a single SFDBA microcrystal marked by a red dotted line. h) XRD patterns of the as-prepared SFDBA microcrystals (top) and the standard powder spectrum based on the single crystal data by using the MERCURY software (bottom).

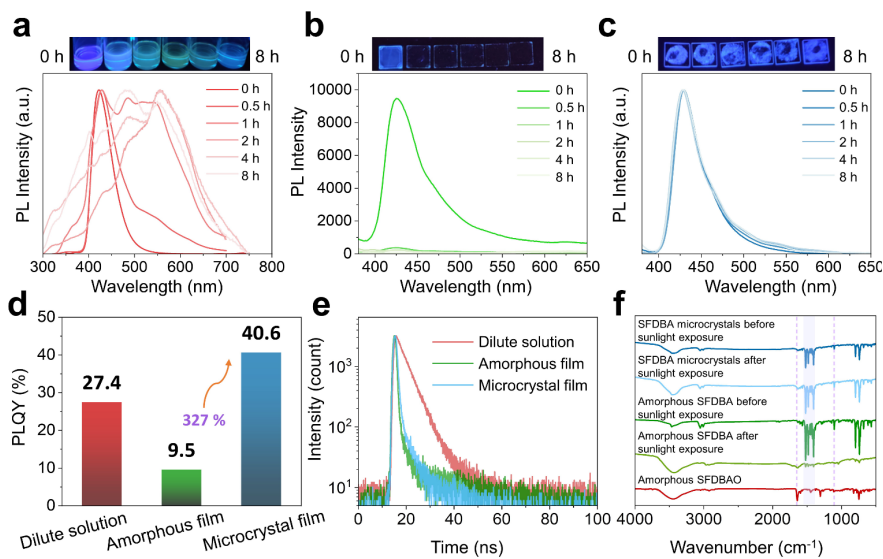


**Figure 3.** The luminescent properties and photooxidation stabilities of SFDBA with different aggregation states. The PL emission spectra evolution of exposed to sunlight for different time intervals: a) dilute solution, b) amorphous film and c) microcrystal film; upper: the corresponding photographs of these samples under 365 nm UV irradiation. d) PLQY of SFDBA with different aggregation states. e) The transient fluorescence decays of SFDBA with different aggregation states at 300 K. f) The FT-IR spectra of SFDBA amorphous film and microcrystal film before and after sunlight exposure for 8 h.

photos are consistent with the spectral results. As reported previously, photo-sensitive naphthylamines of SFDBA tend to be excited and interact with oxygen to form multiple excited state species and radical cation species, generating *5H-spiro[dibenzo[*c,h*]-*a*-*crdine-7,9'*-*uoren*]-5-one* (SFDBAO) as a primary oxidation product, which is able to be further oxidized.<sup>[29]</sup> The calculated emissions of SFDBA and SFDBAO in gas phase is at 415 nm and 544 nm (Table S5), respectively, which is consistent with the experimental emissions. In Figure 3b, the initial SFDBA amorphous film exhibits a PL emission at 426 nm, however, the luminescence is quenched just after half an hour sunlight irradiation. The rapid fluorescence decline indicates the generation of radical cation species in the photooxidative process, which can act as electron acceptors to quench the singlet state even at low concentrations through an effective charge transfer.<sup>[30-32]</sup> The color of the amorphous films after 2 h sunlight irradiation varies from white to a distinct red, and the corresponding thin-layer chromatographic (TLC) analysis confirms that SFDBAO (red dots) is already formed at that point (Figure S4a). The emission spectra of microcrystal films are almost unchanged during the 8 h irradiation by sunlight, still exhibiting an obvious blue light centered at 429 nm, as displayed in Figure 3c. The appearance of the SFDBA microcrystal films keeps invariable white crystal powder without the formation of red SFDBAO, further proved by TLC analysis (Figure S4b). The corresponding XRD patterns in Figure S5 also confirm the stability of the crystalline structure of SFDBAO microcrystal films. The photoluminescence quantum efficiency (PLQY) results of SFDBA in different aggregation states in Figure 3d show that the PLQY value of microcrystal film is the highest (40.6%), which is 48% higher than SFDBA dilute solution and 327% higher than SFDBA amorphous film. The room-temperature-dependent (300 K) transient fluorescence decay curves measured in Figure 3e reveal that the three different aggregation states of SFDBA all display a fluorescent decay character with a nanosecond level (dilute solution: 4.50 ns; amorphous film: 3.06 ns; microcrystal film: 1.88 ns). The Fourier transform infrared (FT-IR) spectra of SFDBA amorphous and microcrystal films in Figure 3f indicate that the spectra are barely changed in the microcrystal film before and after sunlight exposure. However, the amorphous film after sunlight exposure shows an infrared absorption at 1640  $\text{cm}^{-1}$  which can be attributed to the C=O stretching vibration on ketone moieties, while the original C-N stretching vibration and N-H bending vibration at 1099  $\text{cm}^{-1}$  and 1515  $\text{cm}^{-1}$  respectively are disappeared,

demonstrating the SFDBA amorphous film has been oxidized. Based on the above results, a significant improvement in the photooxidation stability and luminescence of SFDBA microcrystal film compared with its amorphous phase is achieved.

To disclose the stability promotion mechanisms, the evolution of the luminescence imaging of SFDBA crystal under different sunlight exposure time intervals is recorded with a fluorescence microscope. The single crystal of SFDBA with larger size (width: 108  $\mu\text{m}$ ) as shown in Figure 4a was adopted for clear observation. The whole SFDBA crystal after 2 h sunlight radiation exhibits a distinct blue light except the corner in the upper right, the light of which is tinted green (Figure 4b). As sunlight radiation prolonged to 4 h, the edges of the crystal exhibit a faint green glow (Figure 4c). Under sunlight irradiation for 8 h, the outline of SFDBA crystal is clearly delineated by green emission, while the main body remains blue emission (Figure 4d). The emergence and extension of green emission confirms that the oxidation process of SFDBA crystal starts at the corner and the edge. Therefore, the principle scheme in Figure

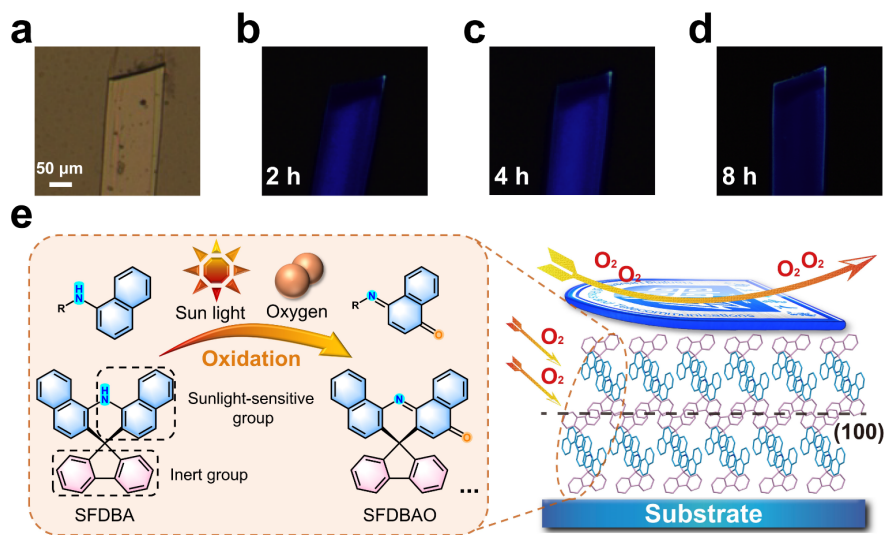


**Figure 4** The mechanism investigation of the photooxidation stability of SFDBA crystal. The images of SFDBA crystal exposed to sunlight for different time intervals: a) 0 h under optical microscope; b) 2 h, c) 4 h, and d) 8h under fluorescence microscope. e) The possible oxidation intermediates and products during the self-sensitization process. f) Schematic illustration of the encapsulation strategy.

4e demonstrates that the sunlight-sensitive naphthylamines are under the protection of closely packed fluorenyl groups as a sterically hindered “armor”, so that the oxygen molecules cannot invade into the largest (100) plane but to attack the narrow lateral face. Further, the calculated Fukui electrophilic functions of the SFDBA molecule and its octamer indicate that the photooxidation active site is located on the acridine ring of the SFDBA molecule and is protected by the “armor” on the other side when the molecule aggregates (Figure S6 & S7). The low-dimensional morphology restricts the entrance of oxygen molecules, further minimizing the detrimental effect of photooxidation.

## Conclusions

In conclusion, a self-encapsulation strategy is displayed by utilizing the ordered arranged stable part of the molecule to form an “armor” for the effective protection of active fragments away from oxygen. The molecular structure design, the molecular packing mode, and the low-dimensional crystal morphology are mutually connected and work together to promote the ultimate oxidative stability of SFDBA materials.

## Experimental

**Experimental Section.** All of chemicals were purchased from J&K Scientific Co. Ltd., and were used without further purification unless otherwise stated.

**Preparation of SFDBA micro/nano-crystals.** The microcrystals of SFDBA were fabricated through reprecipitation method. Typically, 0.5 mg target compounds dissolved in 1 mL THF solution was injected into a 5 mL vigorously stirred water for 5 min, the sample was aging for about 24 h to stabilize the nanostructures. Subsequently, the microcrystals underwent centrifugation and were washed with pure water four times.

**Preparation of SFDBA single crystals.** Single crystals of SFDBA were obtained by the solvent diffusion methods, the growth conditions are manifested in Table S1. Crystallographic information is summarized in Table S2 (these data can also be obtained free of charge from the Cambridge Crystallographic Data Centre: 794132 (SFDBA)).

**Preparation of SFDBA dilute solution.** A certain mass of SFDBA powder was added into 1 mL tetrahydrofuran solution to prepare a solution with a concentration of  $10^{-3}$  mol/L, and then injected 30  $\mu$ L the above solution into 3 mL tetrahydrofuran solution to obtain a dilute solution with a concentration of  $10^{-5}$  mol/L.

**Preparation of SFDBA amorphous film.** A quartz sheet with a size of 1.5\*1.5 cm as the substrate was placed on the spin coater. The tetrahydrofuran solution of the SFDBA with a concentration of 5 mg/mL was dropped to the substrate. The spinning coating speed was 1200 rpm for 30 s, and the acceleration was 400 rpm/s.

**Characterization Details.**  $^1\text{H}$  NMR spectra were measured on a Varian Mercury Plus 400 spectrometer with tetramethylsilane as the internal standard. For scanning electron microscopic (SEM) studies, a drop of 15  $\mu$ L target samples was precipitated on the silicon substrates with the solvent completely evaporated, and then the samples were examined with a field emission SEM (Hitachi S-4800) at an accelerating voltage of 5 kV. The transmission electron microscopy (TEM) and selected-area electron diffraction (SAED) studies were performed in a JEM 2010F JEOL and operated at an accelerating voltage of 100kV. The single crystal data collection was performed at around 100 or 298 K on a Bruker 2000 CCD area detector using graphite-monochromated Mo K $\alpha$  radiation ( $\lambda = 0.71073 \text{ \AA}$ ). All structures were solved by direct methods using SHELXS-2015 and refined against F2 using SHELXL-2015. X-ray diffraction (XRD) patterns were performed on a Bruker D8 X-ray diffractometer with Cu KR radiation ( $\lambda = 1.54050 \text{ \AA}$ ). The operating  $2\theta$  angle ranges from 5 to 30 $^\circ$ , with the step length of 0.025 $^\circ$ . Photoluminescence (PL) emission spectra was measured using a PerkinElmer LS55 spectrophotometer. Photoluminescence quantum efficiency (PLQY) and fluorescence decay curves were measured using a steady/transient fluorescence spectrometer (FLS 920). Fourier transform infrared (FT-IR) spectra was obtained by a PerkinElmer Spectrum Two FTIR spectrometer. The luminescence imaging was taken by Olympus IX71 inverted fluorescence microscope. All the theoretical calculations were performed by using the B3LYP functional with the 6-31G(d) basis set based on their crystallographic data.

#### Supporting Information

The supporting information for this article is available on the WWW under <https://doi.org/10.1002/cjoc.2023xxxxx>.

#### Acknowledgement

This work was supported by the Funded by Natural Science Foundation of Nanjing University of Posts and Telecommunications (NY222157, NY221085), State Key Laboratory of Organic Electronics and Information Display (GZR2022010008), Key Laboratory of Low-dimensional Materials Chemistry of Jiangsu Province (JSKC20022), General Program of China Postdoctoral Science Foundation (2022M711684), General Program of Basic Science (Natural Science) of Colleges and Universities of Jiangsu Province (22KJB430036), National Overseas Study Fund (202008320051), National Key Laboratory (2009DS690095), and the National Natural Science Foundation of China (62288102).

## References

1. Demchenko, A. P.; Photobleaching of organic fluorophores: quantitative characterization, mechanisms, protection. *Methods Appl. Fluores.* **2020**, *8*, 022001.
2. Allen, N. S.; Recent advances in the photo-oxidation and stabilization of polymers. *Chem. Soc. Rev.* **1986**, *15*, 373–404.
3. Mateker, W. R.; McGehee, M.D.; Progress in Understanding Degradation Mechanisms and Improving Stability in Organic Photovoltaics. *Adv. Mater.* **2017**, *29*, 1603940.
4. Boyd, C. C.; Cheacharoen, R. R.; Leijtens, T.; McGehee, M. D. Understanding Degradation Mechanisms and Improving Stability of Perovskite Photovoltaics. *Chem. Rev.* **2019**, *119*, 3418–3451.
5. Stennett, E. M. S.; Ciuba, M. A.; Levitus, M. Photophysical processes in single molecule organic fluorescent probes. *Chem. Soc. Rev.* **2014**, *43*, 1057–1075.
6. Sauer, M.; Heilemann, M. Single-Molecule Localization Microscopy in Eukaryotes. *Chem. Rev.* **2017**, *117*, 7478–7509.
7. Hori, Y.; Hirayama, S.; Kikuchi, K. Development of cyanine probes with dinitrobenzene quencher for rapid fluorogenic protein labelling. *Philos. T. R. Soc. A.* **2017**, *375*, 20170018.
8. Zheng, Y. Y.; Li, M. Y.; Yu, N.; Wang, S. J.; Sun, L. L.; An, X.; Han, Y. M.; Lin, J. Y.; Ding, X. H.; Huang, W. Solution-processed triphenylethylene-fluorene fluorochromes toward deep-blue organic light-emitting diodes: benefits of preventing radical formation. *Mater. Chem. Front.* **2023**, *7*, 267–273.
9. Ghamari, P.; Niazi, R. M.; Perepichka, D. F. Improving Environmental and Operational Stability of Polymer Field-Effect Transistors by Doping with Tetranitrofluorenone. *ACS Appl. Mater. Interfaces* **2023**, *15*, 19290–19299.
10. Song, W.; Lee, J. Y. Degradation Mechanism and Lifetime Improvement Strategy for Blue Phosphorescent Organic Light-Emitting Diodes. *Adv. Opt. Mater.* **2017**, *5*, 1600901.
11. Cui, A. J.; Peng, X. J.; Fan, J. L.; Chen, X. Y.; Wu, Y. K.; Guo, B. C. Synthesis, spectral properties and photostability of novel boron–dipyrromethene dyes. *J. Photoch. Photoblo. A.* **2007**, *186*, 85–92.
12. Hou, L. P.; Zhang, X. Q.; Yao, N.; Chen, X.; Li, B. Q.; Shi, P.; Jin, C. B.; Huang, J. Q.; Zhang, Q. An encapsulating lithium–polysulfide electrolyte for practical lithium–sulfur batteries. *Chem.* **2022**, *8*, 1083–1098.
13. Wang, S. S.; Xu, A. W. Amorphous Calcium Carbonate Stabilized by a Flexible Biomimetic Polymer Inspired by Marine Mussels. *Cryst. Growth Des.* **2013**, *15*, 1934–1942.
14. Zhu, Z. Z.; Li, Z.; Wei, X. X.; Wang, J. J.; Xiao, S. H.; Li, R.; Wu, R.; Chen, J. S. Achieving efficient electroreduction of CO<sub>2</sub> to CO in a wide potential window by encapsulating Ni nanoparticles in N-doped carbon nanotubes. *Carbon.* **2021**, *185*, 9–16.
15. Chang, S.; Wu, X. M.; Li, Y. S.; Niu, D. C.; Ma, Z.; Zhao, W. R.; Gu, J. L.; Dong, W. J.; Ding, F.; Zhu, W. H.; Shi, J. L. A Hydrophobic Dye-Encapsulated Nano-Hybrid as an Efficient Fluorescent Probe for Living Cell Imaging. *Adv. Healthc. Mater.* **2012**, *1*, 475–479.
16. Pradhan, J.; Moitra, P.; Umesh.; Das, B.; Mondal, P.; Kumar, G. S.; Ghorai, U. K.; Acharya, S.; Bhattacharya, S. Encapsulation of CsPbBr<sub>3</sub> Nanocrystals by a Tripodal Amine Markedly Improves Photoluminescence and Stability Concomitantly via Anion Defect Elimination. *Chem. Mater.* **2020**, *32*, 7159–7171.
17. Lin, J. Y.; Liu, B.; Yu, M. N.; Wang, X. H.; Lin, Z. Q.; Zhang, X. W.; Sun, C.; Cabanillas-Gonzalez, J.; Xie, L. H.; Liu, F.; Ou, C. J.; Bai, L. B.; Han, Y. M.; Xu, M.; Zhu, W. S.; Smith, T. A.; Stavrinou, P. N.; Bradley, D. D. C.; Huang, W. Ultrastable Supramolecular Self-Encapsulated Wide-Bandgap Conjugated Polymers for Large-Area and Flexible Electroluminescent Devices. *Adv. Mater.* **2019**, *31*, 1804811.
18. Park, J. S.; Chae, H.; Chung, H. K.; Lee, S. I. Thin film encapsulation for flexible AM-OLED: a review. *Semicond. Sci. Tech.* **2011**, *26*, 034001.
19. Hu, Z.; Han, M. M.; Chen, C.; Zou, Z.; Shen, Y.; Fu, Z.; Zhu, X. G.; Zhang, Y. X.; Zhang, H. M.; Zhao, H. J.; Wang, G. Z. Hollow carbon sphere encapsulated nickel nanoreactor for aqueous-phase hydrogenation-rearrangement tandem reaction with enhanced catalytic performance. *Appl. Catal.*

- B-Environ.* 2022, 306, 121140.
20. Wankar, J.; Kotla, N. G.; Gera, S.; Rasala, S.; Pandit, A.; Rochev, Y. A. Recent Advances in Host–Guest Self-Assembled Cyclodextrin Carriers: Implications for Responsive Drug Delivery and Biomedical Engineering. *Adv. Funct. Mater.* **2020**, *30*, 1909049.
  21. Farcas, A.; Assaf, K. I.; Resmerita, A. M.; Cantin, S.; Balan, M.; Aubert, P. H.; Nau, W. M. Cucurbit [7] uril-based fluorene polyrotaxanes. *Eur. Polym. J.* **2016**, *83*, 256–264.
  22. Wu, X.; Zhu, W. H. Stability enhancement of fluorophores for lighting up practical application in bioimaging. *Chem. Soc. Rev.* **2015**, *44*, 4179–4184.
  23. Niu, D. C.; Li, Y. S.; Qiao, X. L.; Li, Y.; Zhao, W. R.; Chen, H. R.; Zhao, Q. L.; Ma, Z.; Shi, J. L.; A facile approach to fabricate functionalized superparamagnetic copolymer-silica nanocomposite spheres. *Chem. Commun.* **2008**, 4463–4465.
  24. Niu, D. C.; Li, Y. S.; Ma, Z.; Diao, H.; Gu, J. L.; Chen, H. R.; Zhao, W. R.; Ruan, M. L.; Zhang, Y. L.; Shi, J. L. Preparation of Uniform, Water-Soluble, and Multifunctional Nanocomposites with Tunable Sizes. *Adv. Funct. Mater.* **2010**, *20*, 773–780.
  25. Chang, S.; Wu, X. M.; Li, Y. S.; Niu, D. C.; Ma, Z.; Zhao, W. R.; Gu, J. L.; Dong, W. J.; Ding, F.; Zhu, W. H.; Shi, J. L. A Hydrophobic Dye-Encapsulated Nano-Hybrid as an Efficient Fluorescent Probe for Living Cell Imaging. *Adv. Healthc. Mater.* **2012**, *1*, 475–479.
  26. Deng, J.; Deng, D. H.; Bao, X. H. Robust Catalysis on 2D Materials Encapsulating Metals: Concept, Application, and Perspective. *Adv. Mater.* **2017**, *29*, 1606967.
  27. Li, Y. X.; Wang, S. S.; Yu, Y.; Zhang, H.; Wang, W. Y.; Yang, R. Q.; Xie, L. H.; Liu, F.; Lin, Z. Q.; Shi, N. E.; Sun, L. T.; Huang, W.; SMART Design of a Bulk-Capped Supramolecular Segment for the Assembly into Organic Interdigital Lipid Bilayer-Like (ILB) Nanosheets. *Small*. **2017**, *14*, 1703151.
  28. Hu, X. W.; Wang, Y. L.; Zhao, Y.; Wang, G.; Bao, Y.; Xie, C. Solvent Effect on Crystal Structure of Tetracycline Hydrochloride. *Chem. Eng. Technol.* **2013**, *36*, 1355–1358
  29. Wei, Y.; Tang, L.; Zhong, C. X.; Xie, X. M.; Sun, P. J.; Zhang, H.; Zheng, X. P.; Wang, X. L.; Xie, L. H. Photooxygenations and Self-Sensitizations of Naphthylamines: Efficient Access to Iminoquinones. *J. Chem.* **2018**, *2018*, 9180671.
  30. Kazlauskas, K.; Kreiza, G.; Bobrovas, O.; Adomėnienė, O.; Adomėnas, P.; Jankauskas, V.; Juršėnas, S. Fluorene- and benzofluorene-cored oligomers as low threshold and high gain amplifying media. *Appl. Phys. Lett.* **2015**, *107*, 043301.
  31. Dupuis, A.; Wong-Wah-Chung, P.; Rivaton, A.; Gardette, J. Influence of the microstructure on the photooxidative degradation of poly(3-hexylthiophene). *Polym. Degrad. Stabil.* **2012**, *97*, 366–374.
  32. Tomović, A. Ž.; Jovanović, V.P.; Đurišić, I.; Cerovski, V. Z.; Nastasijević, B.; Veličković, S. R.; Radulović, K. Žikić, R. Fast photoluminescence quenching in thin films of 4,4'-bis(2,2-diphenylvinyl)-1,1'-biphenyl exposed to air. *J. Lumin.* **2015**, *167*, 204–210.

---

Manuscript received: XXXX, 2023 Manuscript revised: XXXX, 2023 Manuscript accepted: XXXX, 2023 Accepted manuscript

---

## The Authors

---

After acceptance, please insert a group photo of the authors taken recently.

**Left to Right:** Authors Names

---

## Entry for the Table of Contents

---

“Steric armor” strategy of blue fluorescent emitters to against oxygen-induced degradation Sha-Sha Wang, Ji

---